Supporting Information for

Z-scheme Al$_2$SeTe/GaSe and Al$_2$SeTe/InS van der Waals heterostructures for photocatalytic water splitting

Shaoying Guo[1,2,*†], Zhou Cui[3†], Yanhui, Zou[1] and Baisheng Sa[3,**]

[1]*School of Pharmacy, Fujian Health College, Fuzhou, Fujian 350101, P. R. China*
[2]*Fujian Provincial Key Laboratory of Pollution Control & Resource Reuse, Fujian Normal University, Fuzhou 350003, P. R. China*
[3]*Multiscale Multiscale Computational Materials Facility & Materials Genome Institute, School of Materials Science and Engineering, Fuzhou University, Fuzhou 350108, P. R. China.*

Corresponding Authors: gshy1511@126.com (S. Guo); bssa@fzu.edu.cn (B. Sa).

[†]These authors contributed equally to this work.

Table S1 The binding energies (E_b) of the heterostructures between different stacking configurations

Stacking configurations	0° (meV/Å²)	60° (meV/Å²)	120° (meV/Å²)	180° (meV/Å²)	240° (meV/Å²)	300° (meV/Å²)
Al$_2$SeTe/GaSe	-11.74	-16.74	-16.57	-16.65	-16.51	-11.77
Al$_2$TeSe/GaSe	-10.73	-15.76	-15.65	-15.57	-15.71	-10.77
Al$_2$SeTe/InS	-11.40	-16.57	-16.69	-16.60	-16.15	-11.44
Al$_2$TeSe/InS	-10.33	-15.61	-15.80	-15.62	-15.59	-10.36

Table S2 The formation energies (E_f) of the heterostructures between different stacking configurations.

Stacking configurations	0° (eV)	60° (eV)	120° (eV)	180° (eV)	240° (eV)	300° (eV)
Al$_2$SeTe/GaSe	-0.111	-0.176	-0.174	-0.175	-0.174	-0.112
Al$_2$TeSe/GaSe	-0.098	-0.164	-0.162	-0.161	-0.163	-0.099
Al$_2$SeTe/InS	-0.150	-0.219	-0.221	-0.220	-0.218	-0.150
Al$_2$TeSe/InS	-0.135	-0.206	-0.209	-0.206	-0.206	-0.136

Table S3 The lattice constants, layer distances and band gaps of Al$_2$SeTe/GaSe, Al$_2$TeSe/ GaSe, Al$_2$SeTe/InS and Al$_2$TeSe/InS heterostructures

Heterostructure	Lattice constant (Å)	Layer distance (Å)	Band gap (eV)
Al$_2$SeTe/GaSe	3.869	3.44	1.69
Al$_2$TeSe/GaSe	3.871	3.26	1.77
Al$_2$SeTe/InS	3.926	3.29	1.53
Al$_2$TeSe/InS	3.927	3.11	1.66

Al$_2$SeTe/GaSe	3.869	3.44	1.69
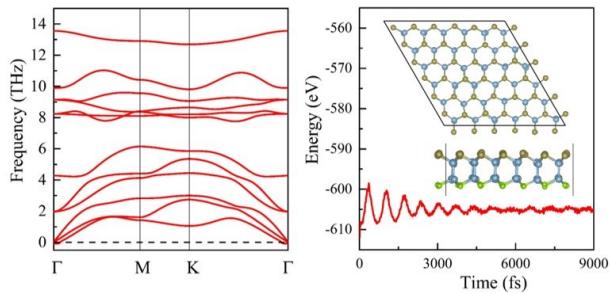
Fig.S1 The phonon dispersion curves and AIMD simulations of Al$_2$SeTe monolayer.
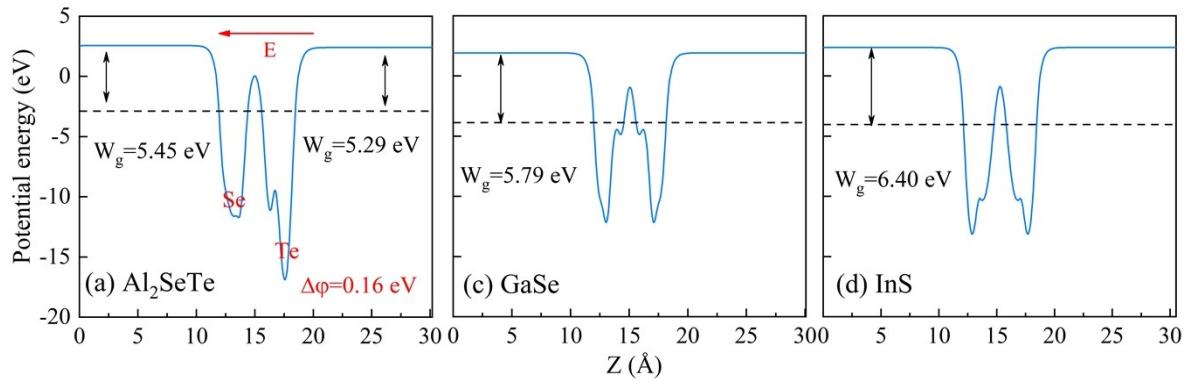
Fig.S2 The planar-averaged electrostatic potential for (a) Janus Al$_2$SeTe, (b) GaSe and (c) InS monolayers along the z-direction.
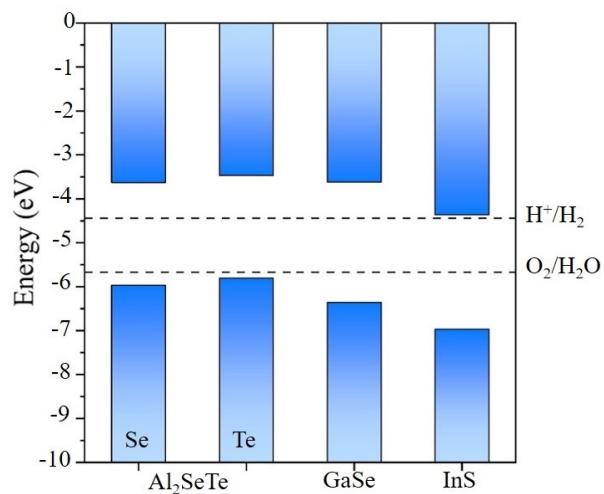
**Fig. S3** The band edge positions of the Janus Al_2SeTe, GaSe and InS monolayers.
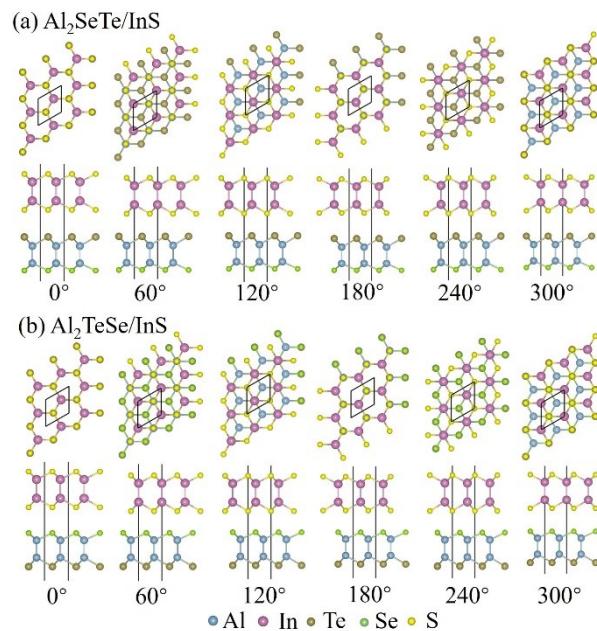
Fig.S4 Top and side views of (a) Al_2SeTe/InS and (b) Al_2TeSe/InS heterostructures with different stacking configurations.
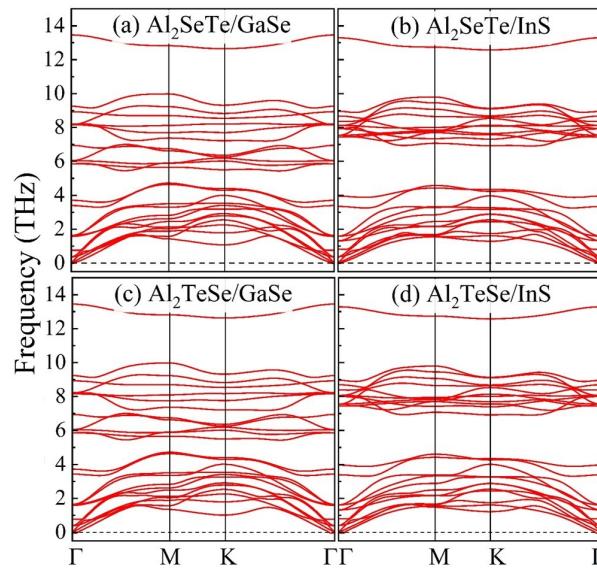
Fig. S5 The phonon dispersion curves of (a) Al$_2$SeTe/GaSe, (b) Al$_2$SeTe/InS, (c) Al$_2$SeTe/GaSe and (d) Al$_2$TeSe/InS heterostructures.
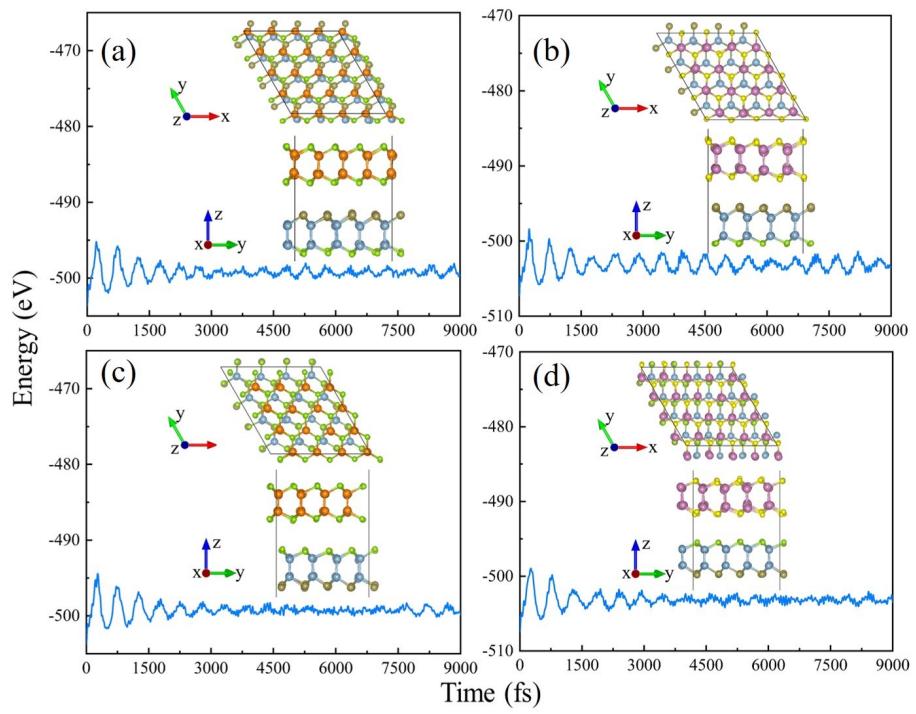
Fig. S6 The AIMD simulations of (a) Al$_2$SeTe/GaSe, (b) Al$_2$SeTe/InS, (c) Al$_2$TeSe/GaSe and (d) Al$_2$TeSe/InS heterostructures with 300 K.
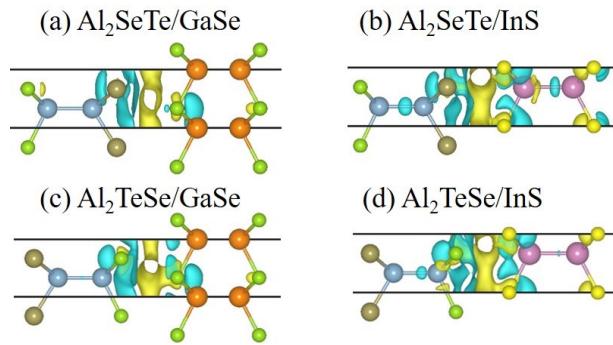
Fig. S7 The 3D isosurface plots for the charge density difference of (a) Al$_2$SeTe/GaSe, (b) Al$_2$SeTe/InS, (c) Al$_2$TeSe/GaSe and (d) Al$_2$TeSe/InS heterostructures. The isovalue is set to 0.00005 e·Å^{-3}. The blue and yellow regions represent the loss and accumulation of charges.
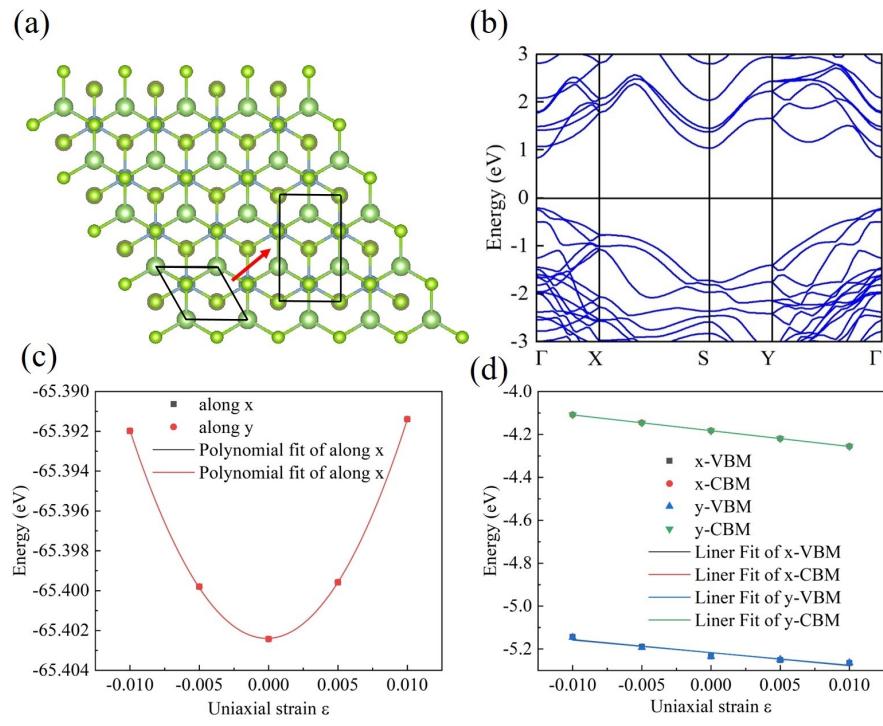
**Fig. S8** The orthorhombic (a) lattice structure, (b) band structure of Al$_2$SeTe/GaSe heterostructure, (c) total energy and (d) band edge positions of Al$_2$SeTe/GaSe as a function of the uniaxial strain ε along both the zigzag (x) and armchair (y) directions.
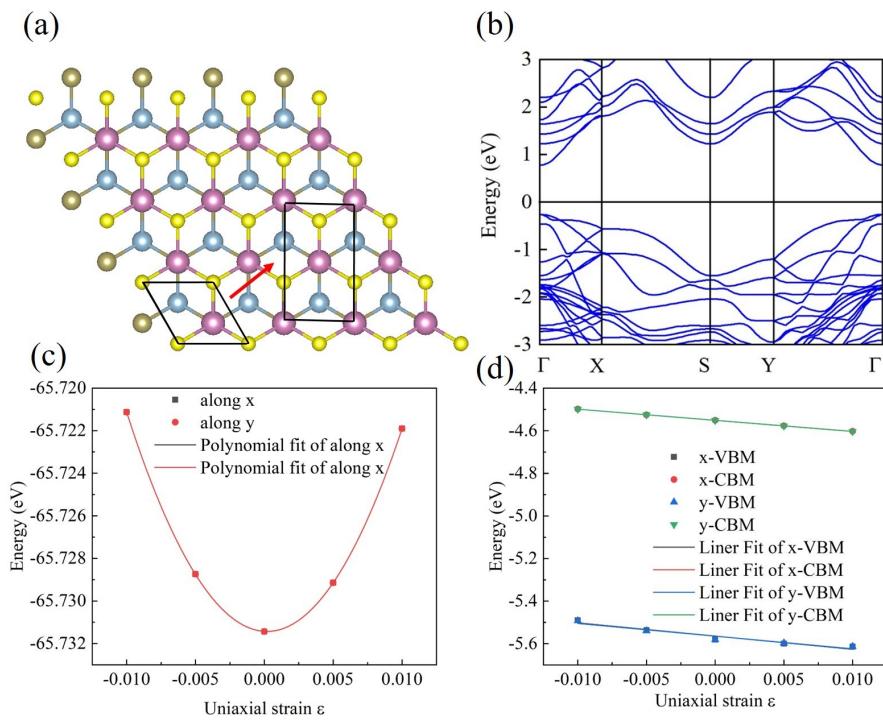
**Fig. S9** The orthorhombic (a) lattice structure, (b) band structure of Al$_2$SeTe/InS heterostructure, (c) total energy and (d) band edge positions of Al$_2$SeTe/InS as a function of the uniaxial strain ε along both the zigzag (x) and armchair (y) directions.
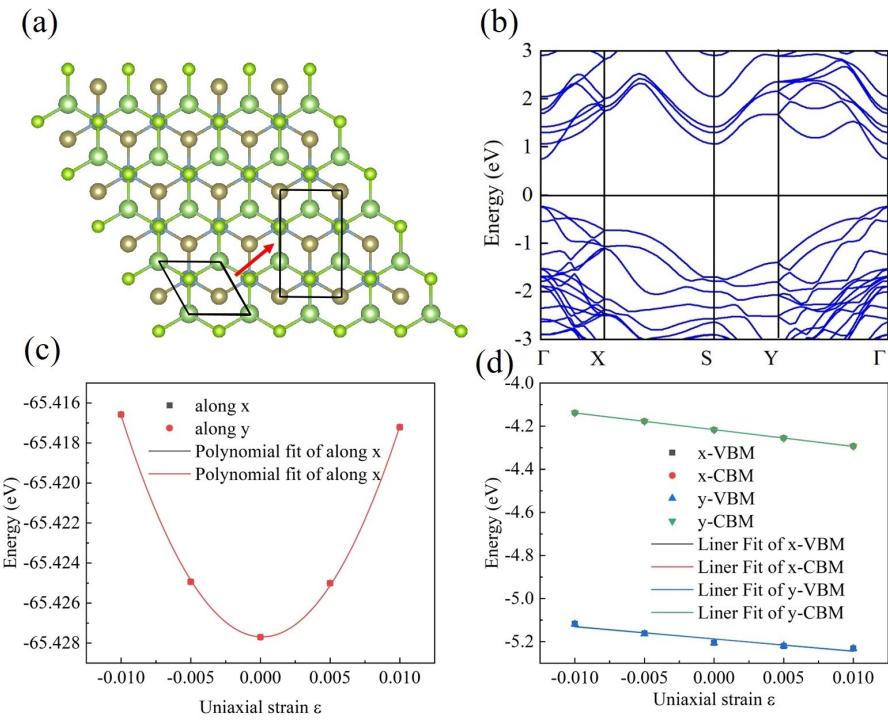
Fig. S10 The orthorhombic (a) lattice structure, (b) band structure of Al$_2$TeSe/GaSe heterostructure, (c) total energy and (d) band edge positions of Al$_2$TeSe/GaSe as a function of the uniaxial strain ε along both the zigzag (x) and armchair (y) directions.
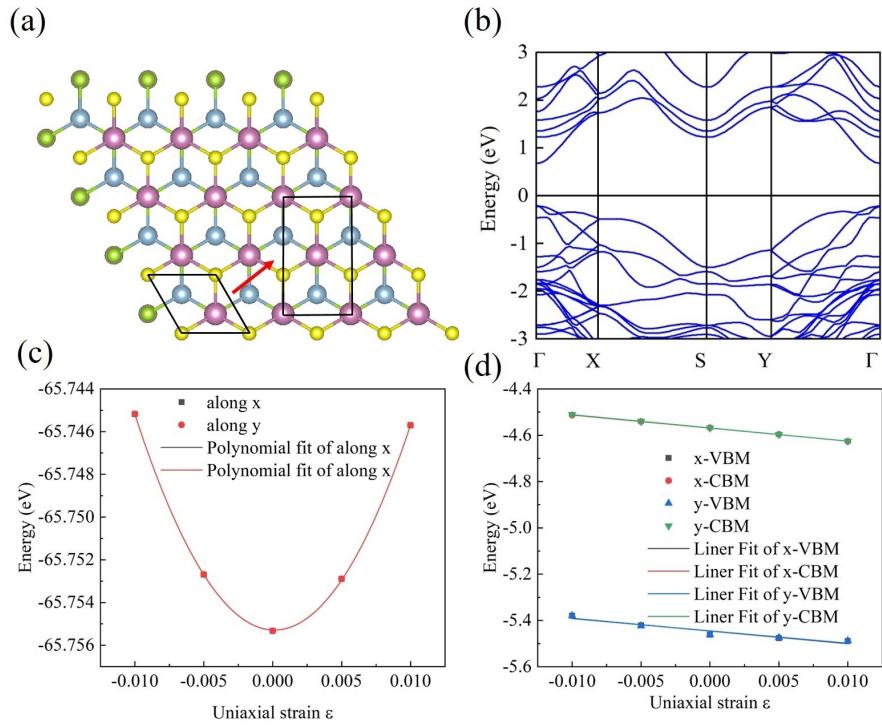
Fig. S11 The orthorhombic (a) lattice structure, (b) band structure of Al$_2$TeSe/InS heterostructure, (c) total energy and (d) band edge positions of Al$_2$TeSe/InS as a function of the uniaxial strain ε along both the zigzag (x) and armchair (y) directions.